FLOW STRUCTURES AND HEAT TRANSFER ENHANCEMENT ON ASYMMETRIC DIMPLES

Johann Turnow*, **Nikolai Kornev**
Institute of Modeling and Simulation
Faculty of Mechanical Engineering and Shipbuilding
University of Rostock
Albert-Einstein-Str. 2
18059 Germany
*johann.turnow@uni-rostock.de

Egon Hassel
Institute of Technical Thermodynamics
Faculty of Mechanical Engineering and Shipbuilding
University of Rostock
Albert-Einstein-Str. 2
18059 Germany

ABSTRACT

Numerical and experimental investigations of fully turbulent flow over an asymmetric dimple with a geometric ratio of dimple depth to diameter of $t/D = 0.26$ in a narrow channel have been performed to identify vortex structures and its influence on heat transfer enhancement at Reynolds number $\mathrm{Re}_D = 40000$ based on the dimple print diameter. The inclination angle of the asymmetric cavity is varied from $0°$ to $90°$ towards the main flow direction. Every $15°$ step the velocity profiles and pressure distribution obtained from LES are compared to parallel conducted experiments in a closed water test channel. Unsteady effects and vortex structures are analyzed and have been opposed to results for a symmetric dimple. Further, the effect of vortex structures on local heat transfer rates are determined and are quantified in reference to the values for a smooth surface. Integral results show best thermo-hydraulic performance for dimples aligned $45°$ to the flow direction.

INTRODUCTION

Since reduction of energy plays a more and more decisive role, vortex enhancement of heat transfer caused by turbulators is currently used in modern heat exchangers. At present several geometries like ribs, fins or dimples have been thoroughly investigated with the aim to improve the heat exchange at a minimum hydraulic loss. It has been shown by many authors (see Isaev SA (2003), Ligrani P.M. (2003)) that concave formed dimples in comparison to other conventional methods show the best thermo-hydraulic performance defined as the ratio between the heat transfer and the pressure loss. Especially with respect to the pressure loss this innovative cooling method shows major advantage as compared to existing conventional methods. The vortices on ribs and fins, which are necessary to mix the fluid, are created through the flow separation on protruding elements what results in a high flow resistance. The vortices on dimpled surfaces are created inside of concave cavities. Since there is no blockage of the channel the additional resistance is minimum. Moreover it has been proved, that the dimples show best effectivity when the flow is turbulent (Ligrani P.M. (2003)). However, since the for the common dimples with a ratio of depth to dimple print diameter of $t/D = 0.2-0.3$ recirculation zones are present, the flow inside the dimple is complicated and it is still not completely understood. Published results have focused on integral values for heat and mass transfer using time averaged methods like RANS whereas unsteady processes and their influence on heat transfer enhance have not been thoroughly investigated using time resolved experimental and numerical methods. Hence, the structure of evolving vortices created within dimples remains not quite clear especially when the flow is in the turbulent regime. Since the form of the vortex has a strong impact on the heat transfer the deep understanding of physics inside of the dimple is important for the further improvement heat exchanger efficiency.

The first investigations of unsteady effects for turbulent flow over a single dimple spherical dimple were performed by Gromov et al. (1986) who presented the picture of vortex formations. A more detailed experimental investigation has been performed by Terekhov et al. (1997) who documented periodical outbursts of vortices from downstream rim using hydrogen bubbles. Transverse oscillations of the outbursts with low ($\omega < 1Hz$) and high frequency ($\omega > 1Hz$) were observed at the Reynolds numbers up to $\mathrm{Re}_D = 40000$. Analysis of instantaneous pictures of the flow revealed a consequent process of generation of regular vortices in the recirculation zone, their shedding downstream resulted in the formation of staggered rows of vortices. These first valuable observations have been quantified by Turnow J. (2010) using modern non-intrusive measurement techniques and advanced LES technologies. Strong asymmetric structures with periodic changing of its direction towards the main flow direction in a total symmetric dimple could be identified using Proper Orthogonal Decomposition (POD) method applied on velocity and pressure fields. Furthermore the asymmetric structures and its oscillations with a frequency of $f = 0.2Hz$ have been confirmed using LDV and time resolved pressure measurements inside and out side of the cavity. Analysis of heat transfer

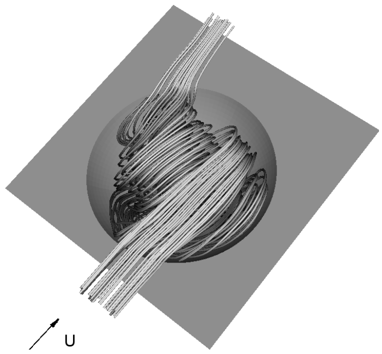

Figure 1: Asymmetric flow structure in a single spherical dimple at $Re_D = 40000$.

showed positive influence of the asymmetric structure since it steadily transfers the hot fluid from the cavity into the main flow. For a fully developed temperature profile in front of the dimple a maximum increase of heat transfer of $\mathrm{Nu}/\mathrm{Nu}_0 = 1.67$ could be observed at $\mathrm{Re}_D = 40000$.
The most detailed experimental studies of unsteady flow characteristics of dimples arranged in a staggered array has been performed by (Mahmood G.I. (2004); Ligrani P.M. (2003)). Flow visualization by smoke patterns revealed a primary vortex pair generating periodically in the center of the hole for moderate Reynolds numbers. Additionally to the primary vortex pair, two secondary vortices arise at the spanwise edges of each dimple inducing vortex structures elongated in streamwise direction which are advantageously in terms of heat transfer enhancement. Furthermore, for dimples with a depth to diameter ratio of $t/D \geq 0.22$ a significant augmentation of heat transfer is documented, when dynamic vortex structures with transversal oscillations occur around dimple area. Nevertheless, the presented smoke observations could only be performed for low Reynolds numbers. In contrast, vortex structures for the fully turbulent flow over a dimple package in a narrow channel published by Turnow J. (2012) showed no coherent structures in the flow and temperature field. Moreover, the strong asymmetric structures as observed for the single dimple could not be confirmed. However, the good performance for a maximum heat transfer enhancement of $\mathrm{Nu}/\mathrm{Nu}_0 = 2.01$ compared to a smooth surface could be identified using LES fields. The vortex structures generated within the shear layer between recirculating and main channel flow avoid a stable recirculation zone for the most effective dimple with a geometric ratio of $t/D = 0.26$. Therefore, the fluid within the cavity is permanently mixed and hot recirculation zone is prevented.

The idea of the present investigation is to force the asymmetric flow structures observed for a single spherical dimple with application of asymmetric formed dimples. In a first step the flow characteristics and integral values of turbulent flow over a single asymmetric dimple with varying inclination angles towards the main flow are studied.

EXPERIMENTAL SETUP

Experimental investigations have been performed in a closed water loop channel schematically presented in Fig. 2. Main parts of the test rig are the head tank with an overflow weir inside, a settling chamber, the converging nozzle (contraction) followed by the test section and a back tank with a metering system. Further a water reservoir, main pump, pipelines and four controlling valves are placed between each device to ensure stable water levels. Water is pumped from the reservoir into the head tank by the main pump which can be additionally tuned to control the mass flow rate. Insight the main tank a weir is installed to reduce turbulence caused by the water pump. In addition an overflow pipe is placed at a predefined height into the head tank to provide a constant water level. The advantage of this setup construction is that a constant water level is ensured in the head tank providing flow with a constant flow rate and a low level of turbulence inside the test section. The rectangular test channel section behind the converging nozzle has the dimension in terms of channel width B, channel height H and total length L of $200mm \times 15mm \times 1340mm$. To provide visual access the test section was made of acrylic glass. To determine the pressure loss inside the test section several sensors have been placed at the lower surface of the channel. Bore holes with an inner diameter of 0.8mm are drilled into the test section and are connected via stable plastic tubes with an inner diameter of $3.5mm$ to a measurement chart to determine the static pressure loss. Laser Doppler Velocimetry (LDV) technique as non-invasive method is applied for the velocity measurements. The 2D Neodym-YAG Laser with a wavelength of $532nm$, $12mW$ power and a focal length of $400mm$ was mounted on a steering unit for exact positioning of the focal point with a position accuracy of 0.1mm. The LDV system is a beam forward scattering system with a combined counter and tracker signal processor. Measurements could not be obtained close to the walls in order to determine the wall shear stresses due to the size of the control volume of the focal point and the impact of reflections. However, at each measurement point the signal representing the velocities was sampled over 10000 times (Bursts) in order to ensure a sufficient statistic. The asymmetric dimple has been placed on a circle plate about 650mm from the inlet in order to ensure a fully developed velocity profile.

NUMERICAL METHOD

Large Eddy Simulations (LES) have been performed based on a 3-D finite volume method. The filtered transport equations are solved on a non staggered Cartesian grid, the discretisation in space and time of the quantities at the cell faces is of second order using central differencing scheme. The LES equations are obtained by filtering the continuity equation, the Navier-Stokes equations and the transport equation for the non-dimensional temperature θ at the filter

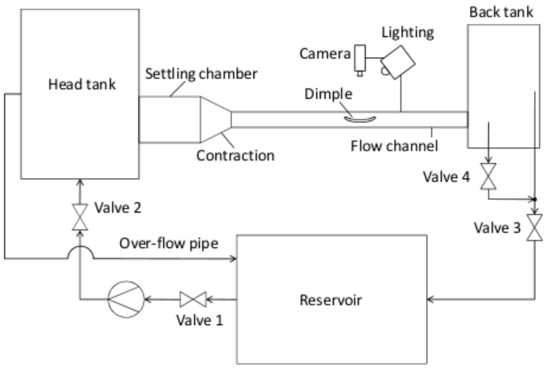

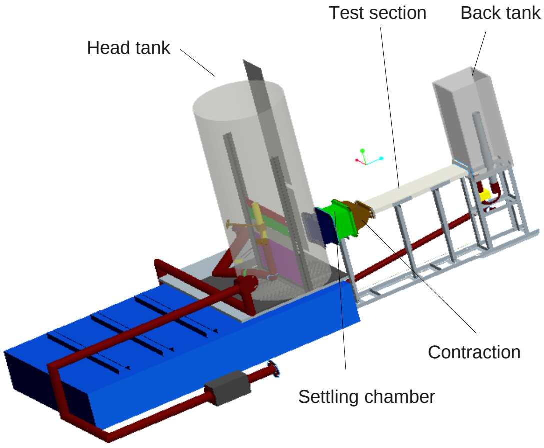

Figure 2: Flow chart and sketch of the experimental bench.

width $\widetilde{\Delta}$:

$$\frac{\partial \widetilde{u}_i}{\partial t} + \frac{\partial \widetilde{u}_j \widetilde{u}_i}{\partial x_j} = -\frac{1}{\rho}\frac{\partial \widetilde{P}}{\partial x_i} + \frac{\partial}{\partial x_j}\left[\nu\left(\frac{\partial \widetilde{u}_i}{\partial x_j} + \frac{\partial \widetilde{u}_j}{\partial x_i}\right) - \tau_{ij}\right], \tag{1}$$

$$\frac{\partial \widetilde{\theta}}{\partial t} + \frac{\partial \widetilde{u}_j \widetilde{\theta}}{\partial x_j} = \frac{\partial}{\partial x_j}\left[\frac{\nu}{\mathrm{Pr}}\frac{\partial \widetilde{\theta}}{\partial x_j} - J_j^{SGS}\right]. \tag{2}$$

The unclosed subgrid stress tensor $\tau_{ij} = \widetilde{u_i u_j} - \widetilde{u}_i \widetilde{u}_j$ and the subgrid contribution to the scalar dynamics $J_j^{SGS} = \widetilde{\theta u_j} - \widetilde{\theta}\widetilde{u}_j$ are modeled in terms of the filtered quantities $\widetilde{u}_i$ and $\widetilde{\theta}$ using the localized dynamic mixed model (LDMM) (Zang Y. (1993)). In Eq. 2 the non-dimensional temperature θ is defined as $(\theta = (T - T_{lowerwall})/(T_{lowerwall} - T_{upperwall}))$ and further treated as a passive scalar without buoyancy effects. The molecular Prandtl number Pr was set to $\mathrm{Pr} = 0.7$, whereas in LES the turbulent viscosity ν_t and the turbulent Prandtl number Pr_t are determined dynamically in space and time using LDMM.

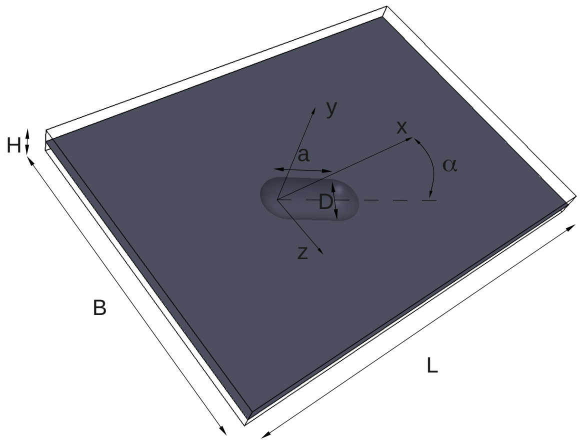

Figure 3: Computational domain of the channel with a single spherical dimple inserted at the lower wall.

COMPUTATIONAL GRID AND BOUNDARY CONDITIONS

The computational domain is presented in Fig. 3. The channel length L, height H and width B was set to $8.9D \times 0.326D \times 6.5D$. The diameter D of the dimple with a sharp edge was kept constant at $D = 46mm$, whereas the dimple depth t has been defined to $t = 0.26D$ and the length between the two half circles to $a = 1D$. Periodic boundary conditions were applied in homogeneous spanwise direction and no slip boundary conditions were enforced on the lower and the upper channel walls. LES inlet conditions were specified using the precursor method where a periodic channel flow was calculated in front of the computational domain. The fluctuations of the channel flow have been used as inlet conditions of the computational domain to ensure correlated velocity and temperature fields in space and time. To drive the flow with a certain velocity U_b, the overall losses within the channel were calculated and simply added as the driving force to the momentum equation.

In order to establish the grid independence of the LES model a series of calculations have been carried out. On its base a curvilinear grid consisting of 4.5 mio was chosen for detailed investigations. It should be noted that the domain size should be chosen carefully to capture typical velocity and temperature structures. To reduce numerical residuals due to strong mesh deformation, a new method based on mesh motion technique is applied. Therefore, in a first way the mesh is constructed for a smooth channel and afterwards stretched onto the curved surface using mesh diffusion equation (see Jasak H. (2006)). Hence, the streamlines nearly follow flow field and strong mesh deformations are avoided.
The number of cells in- and outside the dimple was increased to resolve the main vortex structures arising from the dimple surface. The stretching of grid cells was set to satisfy the condition $y^+ \leqq 1$ for the fist grid point. Therefore, the first grid points are always located inside the laminar sublayer.

RESULTS

Validation

For validation, reference and establishment of the grid independency a series of calculations of a turbulent channel flow with the dimension of $4.66H \times H \times 4.66H$ with smooth walls have been performed. Two Reynolds numbers $\mathrm{Re}_D = U_{bulk}D/\nu = 20000$ and $\mathrm{Re}_D = 40000$ were considered which are equivalent to the Reynolds numbers $\mathrm{Re}_H = U_{bulk}H/\nu = 6521$ and $\mathrm{Re}_H = 13042$ based on the channel height H. The total number of grid points used for the channel flow is $256 \times 80 \times 256 \approx 5.25 \cdot 10^6$. In spanwise and streamwise direction homogeneous grid stretching is used normal to the wall with the first grid point is placed at $y^+ = 0.4$. Table 1 summarizes the results for the skin-friction coefficient C_f obtained from numerical simulation and our pressure measurements.

Table 1: Comparison of the skin-friction coefficient C_f obtained from LES and experiment with empiric correlations from Dean for a turbulent channel flow at $\mathrm{Re}_H = 6521$ and $\mathrm{Re}_H = 13042$.

		C_f	Dean
$\mathrm{Re}_H = 6521$	LES	0.0671	0.06835
	Exp	0.0692	
$\mathrm{Re}_H = 13042$	LES	0.0591	0.05748
	Exp	0.0602	

The skin-friction coefficients obtained from experiment and simulations show very good agreement with empirical correlation given by Dean $C_f = 0.06138\ \mathrm{Re}^{-1/4}$. Comparison of LES data for the heat transfer rates with the empiric correlations of Gnielinsky

$$Nu = \frac{(\xi/8)\ \mathrm{RePr}}{1 + 12.7\sqrt{\xi/8}\ (\mathrm{Pr}^{2/3} - 1)}(1 + (d_h/l)^{2/3}) \qquad (3)$$

and Dittuis-Boelter $Nu = 0.023\ \mathrm{Re}^{0.8}\ \mathrm{Pr}^{0.4}$ is summarized in Table 2.

Table 2: Comparison of Nusselt number Nu of LES and empiric correlations from Gnielinsky and Dittuis-Boelter for a turbulent channel flow at $\mathrm{Re}_H = 6521$ and $\mathrm{Re}_H = 13042$.

		Nu	Boelter	Gnielinsky
$\mathrm{Re}_H = 6521$	LES	23.78	22.39	24.04
$\mathrm{Re}_H = 13042$	LES	38.4	38.97	38.87

The discrepancy does not exceed 1% what underlines the accuracy of the present calculations.

Further numerical results obtained from LES are compared with experimental data obtained from parallel conducted measurements. Figure 4 shows the profile of normalized mean velocity and corresponding r.m.s values obtained from LES and experiments along the channel height at three positions $x/D = 0.0$, $z/D = 0.0$; $x/D = 0.5(\sqrt{2}/2)$, $z/D = 0.5(\sqrt{2}/2)$ and $x/D = 1.0(\sqrt{2}/2)$, $z/D = 1.0(\sqrt{2}/2)$ within in the asymmetric dimple for an inclination angle of 45°. The data obtained for the Reynolds number of $\mathrm{Re}_D = 40000$ are normalized by the bulk velocity U_b.

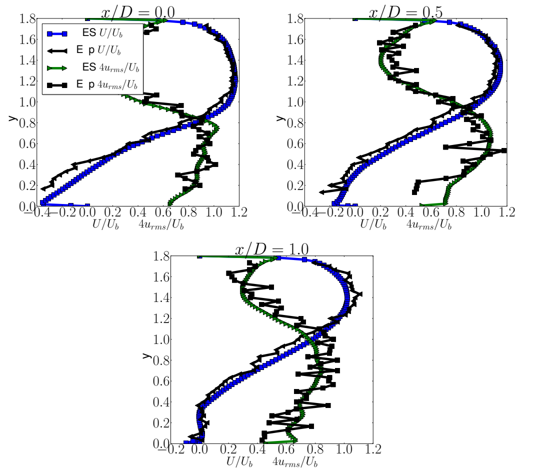

Figure 4: Velocity and rms profiles across the channel height at three positions $x/D = 0.0$, $z/D = 0.0$; $x/D = 0.5(\sqrt{2}/2)$, $z/D = 0.5(\sqrt{2}/2)$ and $x/D = 1.0(\sqrt{2}/2)$, $z/D = 1.0(\sqrt{2}/2)$ at Reynolds number $\mathrm{Re}_D = 40000$ with an inclination angle of 45°.

Numerical results show good agreement with experimental data. Small discrepancy with measurements can be observed in the near wall region inside the cavity. The most probable reason for the discrepancy between theory and experiment in this region are the typical LDV measurements problems in close proximity to the wall due to reflections. The strongest velocity gradients are detected within the shear layer between recirculating and main flow. Vortices generated on the border of the recirculation zone at $y/H \sim 0.8$ produce significant pulsations due to the instability of the shear layer. In addition, the normalized pressure values in terms of $C_p = \Delta pH/(\rho U_b^2/2)$ obtained from experiment and numerics at the bottom centerline are presented in Fig. 5.

The predicted pressure distribution inside and outside the asymmetric dimple agree well with experimental data. Also for other inclination angles (not shown here) the comparison shows good results. A small pressure decrease is observed at the leading edge at $x/D = 0.5$ since the flow becomes separated for all configurations. Further downstream the pressure coefficient C_p experiences an exponential increase equal to measurements. This effect is caused by the stagnation of the main channel flow which attaches the dimple surface. A dramatic pressure loss happens further downstream at $x/D = 1.5$ due to the flow separation where the flow passes over the trailing edge of the dimple. Afterwards the pressure distribution tends to be same as predicted by the correlation for a smooth channel.

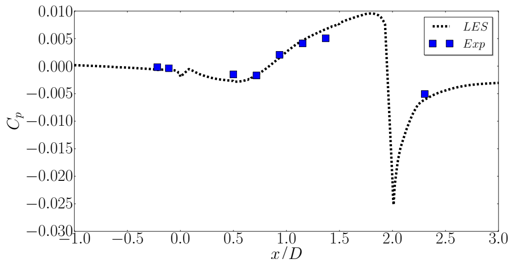

Figure 5: Measured and predicted pressure coefficient C_p along the bottom centerline at Reynolds number $\mathrm{Re}_D = 40000$ with an inclination angle of $45°$.

Vortex structures

The analysis of the transverse motion of the fluid and its influence on heat transfer enhancement for the asymmetric dimple with application of different inclination angles up to $90°$ is done by analyzing time resolved data from LES. As expected, due to the asymmetric form the asymmetric flow structures already observed for the spherical dimple (see Fig. 1) are forced and strengthened. For further explanations the iso-surfaces of instantaneous pressure fields and the corresponding streamlines are presented in the following Fig. 6, 7 and 8.

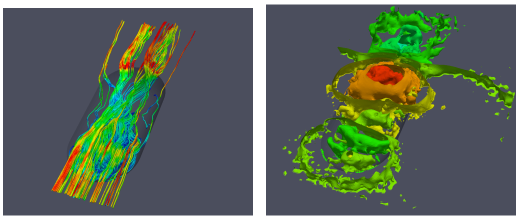

(a) (b)

Figure 6: Streamlines and pressure isosurfaces from instantaneous LES fields for an asymmetric dimple $(0°)$ $Re_D = 40000$.

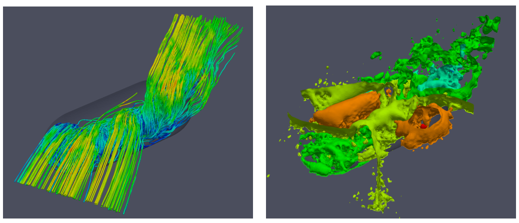

(a) (b)

Figure 7: Streamlines and pressure isosurfaces from instantaneous LES fields for an asymmetric dimple $(45°)$ $Re_D = 40000$.

From streamline patterns it can be seen that the incoming cold fluid strikes the curved surface. The generated vortex located within the dimple dominantly rotates along the

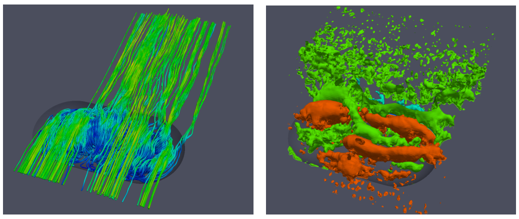

(a) (b)

Figure 8: Streamlines and pressure isosurfaces from instantaneous LES fields for an asymmetric dimple $(90°)$ $Re_D = 40000$.

inclination angle axis due to the asymmetric cavity. Hence, the steadily ejected fluid includes vortex structures elongated in streamwise direction (positive in respect to flow resistance) enhancing heat transfer behind the surface depression. The rotation of the fluid is strictly enforced when the inclination angle is increased up to $60°$. However, for angles higher than $60°$ the streamwise component gets weak and the fluid mainly rotates within the cavity. Moreover, the steady ejection of the hot fluid could not be observed for $\alpha \geq 60°$.
The three dimensional vortex rollup's generated within the shear layer between recirculating and main channel flow can be observed from the pressure iso-surfaces for every dimple configuration due to flow separation at the leading edge. The detailed dynamic motions of the small scale vortex structures arising in the shear layer are especially identified in the animation of the flow field data. Furthermore, it was shown by variation of dimple depth that for a ratio of $t/D = 0.26$, that the fluctuations are still present at the dimple surface avoiding a stable recirculation zone. In respect to heat transfer enhancement those shear layer structures induce fluctuations normal to the dimple surface which can be twice as high as for the smooth surface at its maximum. Further, a second flow separation has been observed at the trailing edge where the fluid is ejected out of the dimple which enhance fluctuations and therefore heat transfer downstream of the dimple.

Heat Transfer

To quantify the heat transfer enhance and resulting flow resistance the values obtained for the asymmetric dimples are compared to data obtained for a smooth channel. Therefore, a rectangular section of $2.5D \times 3.0D$ around the asymmetric dimple was chosen for each configuration. For notice, the values for the Nusselt number have been integrated at the selected surface that heat transfer enhancement due to surface enlargement is excluded. For evaluation of the overall flow resistance the form and friction drag have been calculated at the selected surface. Fig. 9 depicts the comparison of heat transfer and resistance compared to a smooth surface.

The total resistance is gradually increased as the inclination angle α is enlarged. The highest increase of resistance can be found when α is switched from $\alpha = 60°$ to $\alpha = 75°$ which is the result of formation of an large recirculation zone inside the dimple. From analysis of the form and friction forces it can be observed, that the overall resistance is mainly driven by the increase of the form whereas in contrast the friction component permanently decreases

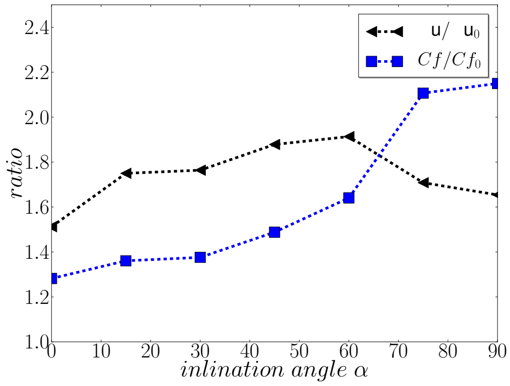

Figure 9: Resistance and heat transfer coefficients compared to values for a smooth channel for different inclination angles at $\mathrm{Re}_D = 40000$.

since the recirculation zone is increasing for larger inclination angles. However, the values of the overall resistance ratio varying from $C_f/C_{f0} = 1.28$ up to $C_f/C_{f0} = 2.14$ are still smaller in comparison to other vortex generators like ribs or fins which can be eight times higher.

With analysis of the integral Nusselt number a steady enhancement is oberserved when the inclination angles is increased up to 60° whereas for α values larger than $\alpha \geq 60°$ the overall heat transfer is decreased. From local Nusselt-number analysis the areas of low heat transfer can be found within the recirculation zone. Within this area the Nusselt number is gradually decreased as α increases up to $\alpha = 60°$. For values larger than $\alpha = 60°$ the recirculation zone becomes stronger and the fluids remains longer inside the cavity. Hence, the temperature of the fluid increases and thus the heat transfer is lowered. Areas of high heat transfer with Nusselt numbers up to eight times higher than for a smooth channel are located near the trailing edge where the cold fluid attaches the dimple surface.

Conclusion

Comparison of numerical results with parallel conducted experiments shows that the LES models are capable of predicting the turbulent flow over an asymmetric dimple in a narrow channel with a satisfactory accuracy.
LES reveal the presence shear layer structures which enhance fluctuations inside the cavity. The same conclusion has been drawn from equivalent LDV measurements. Analysis of flow structures using instantaneous streamlines and pressure iso-surfaces shows clearly the presence of the coherent vortex structures which are inclined with respect to the inclination angle. For Reynolds number $\mathrm{Re}_D = 40000$ it was found that the asymmetric dimple with an inclination angle of $\alpha = 45°$ provides the best thermo-hydraulic performance. Largest heat transfer rates are observed for $\alpha = 60°$, however the increase of flow resistance is higher compared to $\alpha = 45°$. Furthermore, a drastical decrease of heat transfer is obtained for α-values larger than $\alpha \geq 60°$ since the fluid rotates inside the cavity where a defined fluid ejection is not present.

REFERENCES

Isaev SA, Leont'ev, A.I. 2003 Vortex enhancement of heat transfer under conditions of turbulent flow past a spherical dimple on the wall of a narrow channel. *High Temperature* **41** (5), 655–679.

Jasak H., Tukovic Z. 2006 Automatic mesh motion for the unstructured finite volume method. *Transactions of FAMENA* **30** (2), 1–20.

Ligrani P.M., Oliveira M.M., Blaskovich T. 2003 Comparison of heat transfer augmentation techniques. *AIAA J.* **41** (3), 337–362.

Mahmood G.I., Ligrani P.M. 2004 Heat transfer in a dimpled channel combined influences of aspect ratio, temperature, reynolds number, and flow structure. *Int. J. of Heat and Mass Transfer* **45**, 2011–2020.

Turnow J., Kornev N., Isaev S. Hassel E. 2010 Vortex mechanism of heat transfer enhancement in a channel with spherical and oval dimples. *Heat and Mass Transfer* **47** (3), 301–313.

Turnow J., Kornev N., Zhdanov V. Hassel E. 2012 Flow structures and heat transfer on dimples in a staggered arrangement. *Int. Journal of Heat and Fluid Flow* **35**, 168175.

Zang Y., Street R.L, Koseff J.R. 1993 A dynamic mixed subgrid-scale model and its application to turbulent recirculating flow. *Physics Fluids* **12**, 3186–3196.